ACS APPLIED MATERIALS & INTERFACES

Research Article

www.acsami.org

# First-Principles Characterization of the Critical Thickness for Forming Metallic States in Strained $LaAlO_3/SrTiO_3(001)$ Heterostructure

Safdar Nazir and Kesong Yang*

Department of NanoEngineering, University of California, San Diego, 9500 Gilman Drive, Mail Code 0448, La Jolla, California 92093-0448, United States

Supporting Information

**ABSTRACT:** The emerging two-dimensional electron gas (2DEG) at the interface between polar $LaAlO_3$ (LAO) and nonpolar $SrTiO_3$ (STO) provides potential applications in low-dimensional nanoelectronic devices because of its exceptional electron transport property. To form 2DEG in the LAO/STO heterostructure (HS), a minimum thickness of approximately 4 unit cells of LAO is necessary. Herein, we modeled the *n*-type $(TiO_2)^0/(LaO)^{+1}$ HS by depositing $(LAO)_n$ ($n$ = 4, 5, and 6) thin films on the STO substrate and explored strain effects on the critical thickness for forming 2DEG in the LAO/STO HS-based slab systems using first-principles electronic structure calculations. A vacuum layer was added along the [001] direction on the LAO film to resemble the actual epitaxial growth process of the materials. An insulator-to-metal transition is predicted in unstrained $(LAO)_n$/STO systems when $n \geq 5$. Our calculations indicate that O $2p_x/p_y$ states give rise to the surface conductivity, while Ti $3d_{xy}$ states are responsible for the interfacial conductivity. For the tensilely strained HS system, an increased film thickness of LAO ($n \geq 6$) is required to form the 2DEG, and a remarkable shift of O 2p orbitals toward higher energy in LAO layers is found, which is caused by the strain-induced change of the electrostatic potential. For the compressively strained HS system, the critical thickness of LAO film for forming 2DEG is between 5 and 6 unit cells of LAO. In addition, our calculations suggest that the interfacial charge carrier density and magnetic moment can be optimized when a moderate tensile strain is applied on the STO substrate in the *ab*-plane.

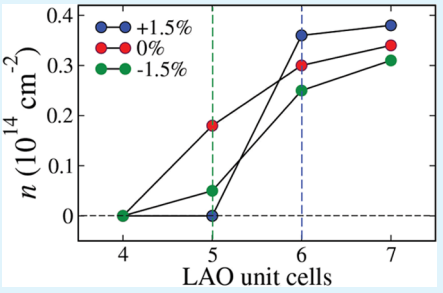


**KEYWORDS:** *2DEG, oxide heterostructure, first-principles, strain effects, critical thickness, charge carrier density*

## 1. INTRODUCTION

The recently discovered 2DEG at the *n*-type $(TiO_2)^0/(LaO)^{+1}$ interface between two wide-band gap insulating oxides, polar $LaAlO_3$ (LAO) and nonpolar $SrTiO_3$ (STO), has become an intensive research topic due to its potential applications in the next-generation nanoelectronics.[1−10] To implement the 2DEG in practical applications of high-performance nanodevices, tunable electron transport properties such as high charge carrier density and mobility are essential. A common technique for tuning material properties of the epitaxially grown film is to apply a mechanical strain. For example, in-plane compressive strain can significantly influence the superconducting transition temperature of the well-known $La_{2-x}Sr_xCuO_4$ superconducting materials[11,12] and the Curie temperature of ferroelectric materials.[13−16] An ordinary band insulator consisting of heavy elements may become a topological insulator under an appropriate strain.[17] Applying a tensile strain can effectively narrow the band gap of STO, enabling it to harvest light from the visible solar spectrum more efficiently.[18] Besides the band gap modification, the charge carrier density and mobility in traditional metal oxide semiconductor field effect transistors can also be tuned via strain engineering.[19−21]

Recent experimental and computational studies both showed that applying an appropriate strain on STO could modify the electron transport properties of 2DEG in STO-based heterostructures (HSs). In experiments, strain on the STO substrate can be achieved by growing it on a single-crystal substrate with different lattice parameters prior to depositing the LAO film. For example, Eom's research team grew the LAO/STO HSs on various substrates and observed a substantial electrical conductivity dependence of the 2DEG on the substrates.[22] They found that the interfacial charge carrier density of the LAO/STO HS system increases when the STO substrate undergoes a strain in the range from −1.5% to +0.5%. Our recent first-principles study supports this conclusion that applying a tensile strain on the STO substrate can significantly increase the interfacial charge carrier density in the LAO/STO HS.[23] This growing body of evidence shows that strain plays a crucial role in tuning the 2DEG of the LAO/STO system. It is already known that, in order to form 2DEG in the perovskite-based HS systems, the thickness of the polar perovskite film must be above a critical value.[1,24] For example, a minimum thickness of approximately 4 unit cells of LAO is necessary to form the 2DEG in the LAO/STO system.[8,24,25] As a result, one may speculate that a different critical thickness may be required to form 2DEG in the strained LAO/STO HSs.

Received: September 16, 2014
Accepted: November 28, 2014
Published: November 28, 2014

  

Actually, Eom's research team found that for the compressively strained LAO/STO HSs the critical thickness of the LAO unit cells increases. In other words, a thicker LAO film of more than 4 unit cells is needed for forming 2DEG in the LAO/STO HS. To elucidate this experimental phenomenon, in this work, we investigated the electronic properties of the $(TiO_2)^0/(LaO)^{+1}$ *n*-type interface in the LAO/STO system and focused on the characterization of the required critical thickness for forming 2DEG using first-principles electronic structure calculations. We first studied the LAO thickness dependence of the formation of the 2DEG in unstrained LAO/STO HS-based slab systems. Next, we explored the influence of biaxial compressive and tensile strain in the *ab*-plane on the critical thickness of the LAO layer for forming 2DEG. In addition, it was found that the biaxial strain plays a substantial role in modifying the 3d orbital occupation of the interfacial Ti atoms, which influence the interfacial charge carrier density and magnetic moment.

## 2. COMPUTATIONAL DETAILS

Our electronic structure calculations were carried out by the Vienna *Ab-initio* Simulation Package (VASP).[26,27] The spin-polarized generalized gradient approximation (GGA)[28] plus on-site Coulomb interaction approach (GGA+*U*) was applied for the exchange-correlation potential with $U$ = 5.8 and 7.5 eV for Ti 3d and La 4f orbitals, respectively. A kinetic energy cutoff of 450 eV and a 10 × 10 × 1 *k*-space grid were used. Structural optimization was taken into account by minimizing the atomic forces up to 0.02 eV/Å. Self-consistency was assumed for a total energy convergence of less than $10^{-5}$ eV. A Gaussian smearing of 0.05 eV was used for density of states (DOS) calculations. A supercell approach was used to model the LAO/STO HS-based slab systems by depositing LAO (4−6 unit cells) thin films on $(STO)_8$ (001) substrates. Herein, it is noticed that a HS-based slab system that contains a vacuum layer is necessary to investigate the critical thickness of the LAO film for forming 2DEG.[6,29] In this work, we added a vacuum layer of about 12 Å along the [001] direction on the LAO layer as proposed in this calculation.[29] As a result, two types of polar discontinuities are present in our supercells. One is at the interface, and the other one is at the surface. The former polar discontinuity occurs between the polar LAO and nonpolar STO, while the latter one occurs between the polar LAO and vacuum. The experimental lattice constants of the LAO and STO were used, leading to a lattice mismatch of approximately 2.97%. The experimental lattice constant of STO of 3.905 Å was fixed in the *ab*-plane to model the HS for all unstrained systems and then was varied to model the strained systems.

## 3. RESULTS AND DISCUSSION

**3.1. Bulk Parent Compounds.** The bulk compounds LAO and STO crystallize in a cubic phase with space group no. 221 ($Pm\bar{3}m$). Our calculated lattice parameters from the standard DFT calculations are in good agreement with the experimental values ($a$ = 3.810 vs 3.789 Å for LAO and $a$ = 3.945 vs 3.905 Å).[1] In contrast, the calculated band gaps from the GGA+*U* approach are underestimated with respect to the experimental values (3.1 vs 5.6 eV for LAO and 2.5 vs 3.2 eV),[1] which is due to the well-known shortcoming of the GGA functional that cannot give an accurate description for the electron−electron correlation-exchange interaction. This underestimation, however, has no influence on our conclusions regarding the discussion of the 2DEG at the LAO/STO system because the Ti 3d electronic states that contribute to the formation of 2DEG can be well reproduced from GGA+*U* calculations.[30,31] As discussed later, our GGA+*U* approach well predicts the 2DEG-related Ti 3d states as well as the critical thickness of the LAO for forming the 2DEG in the unstrained system, which is consistent with the conclusion from hybrid density functional theory calculations.[8]

**3.2. Critical Thickness for Forming 2DEG in Unstrained HS.** First, to examine the critical thickness of LAO films for forming 2DEG in the unstrained LAO/STO HS-based slab system, we modeled the *n*-type LAO/STO HS systems by depositing LAO thin films on the STO substrate stacking along the [001] direction. In this work, we used $(LAO)_n$ to denote $n$ LAO unit cells for convenience. The electronic states near the interface strongly depend on the local structural distortion caused by relaxation,[6,32−34] i.e., the displacement of the atoms near the interfacial region. Therefore, the $(LAO)_n$/STO ($n$ = 4, 5, and 6) HSs were fully relaxed by minimizing their atomic forces in this work. Our structural optimization shows that at the interface Ti−O and Al−O bond lengths along the *c*-axis increase from 0.02 to 0.04 Å and 0.05 to 0.07 Å, respectively, as compared to that in the unrelaxed system. The Al−O bond length along the *c*-axis at the surface layer increases from 0.03 to 0.05 Å, which shows a similar structural relaxation behavior as observed near the interface region. In contrast, only oxygen atoms in the $AlO_2$ surface layer slightly (∼0.01 Å) move toward the vacuum layer as compared to all the other oxygen atoms in LAO and STO sides.[29] In short, a substantial change is found in the LAO side as compared to STO, which is vastly different from periodic LAO/STO HS where a pronounced structural relaxation is seen in the STO side.[35] This conclusion is consistent with the previous computational study on bilayer-type LAO/STO HS-based slab systems in the frame of the LDA+*U* approach, in which the structural relaxation occurs primarily in the LAO side.[36] Similar structural relaxation behavior also occurs in sandwich-type systems.[8,36] For example, Pavlenko et al. studied a STO/LAO/STO sandwich-type system and found small atom displacements only in the interfacial LaO layers.[36] Cossu et al. studied a LAO/STO/LAO sandwich-type system using hybrid density functional calculations and found that buckling effects caused by structural relaxation are stronger for LAO layers and almost negligible for $TiO_2$ interfacial layers.[8] Interestingly, these structural relaxation effects are in good agreement with the experimental observations.[37,38] For instance, by using surface X-ray diffraction techniques, Salluzzo et al. found relatively large cation displacements in the LAO compared with that in the STO,[37] and Pauli et al. observed a much stronger buckling structure in the LAO side than in the STO side.[38]

Regarding the electronic properties, the calculated total DOS for the fully relaxed structures of $(LAO)_4$/STO, $(LAO)_5$/STO, and $(LAO)_6$/STO are shown in Figure 1. For the $(LAO)_4$/STO system with 4 LAO unit cells deposited on the STO substrate, our calculation shows an insulating character with a band gap of 0.15 eV (see Figure 1a). Although not shown here, the LAO/STO systems with fewer LAO layers, i.e., $(LAO)_n$/STO ($n$ = 1, 2, and 3), also show a band gap. However, when the LAO film thickness is increased up to 5 unit cells, the band gap vanishes (see Figure 1b). As discussed later, the metallic states partially come from the Ti 3d states at the interfacial $TiO_2$ layers, indicating the formation of 2DEG. When the thickness of LAO increases up to 6 unit cells, more states

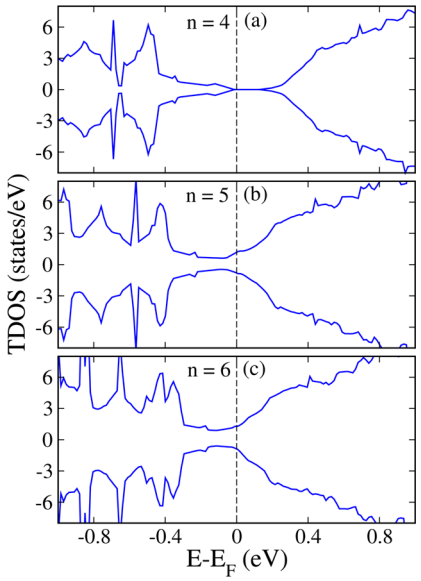


**Figure 1.** Calculated spin-polarized total DOS for the $(LAO)_n$/STO HS-based slab systems. (a) $n = 4$, (b) $n = 5$, and (c) $n = 6$. $n$ refers to the number of LAO unit cells. The vertical dashed line indicates the Fermi level at 0 eV.

emerge near the Fermi level, as shown in Figure 1c. The increased thickness of the LAO film for producing metallic states is consistent with previous results.[6,39] In addition, our electronic structure calculations for these unrelaxed LAO/STO HS systems reveal metallic conducting properties, which is in alignment with previous conclusions.[6] This means that structural distortion has significant effects on the electronic properties of LAO/STO HS-based slab systems. In short, we can conclude that for the *n*-type LAO/STO system a critical thickness of 5 LAO unit cells is necessary to form metallic states on the interface. This result is well consistent with previous conclusions from GGA and hybrid density functional calculations.[6,8] The calculated critical thickness is also in good agreement with experimental findings which reveal that 4 unit cells of LAO film are enough to produce 2DEG in the *n*-type LAO/STO system.[24,40,41]

To understand the origin of the metallic electronic states, we calculated layer-resolved DOS for the $(LAO)_5$/STO model depicted in Figure 2. It shows that O 2p states of the $(LaO)^{+1}$ and $(AlO_2)^{-1}$ layers significantly shift toward higher energy when these layers move from the interfacial region to the vacuum layer. In particular, at the $(AlO_2)^{-1}$ surface layer, the O 2p states cross the Fermi level, suggesting that the surface $(AlO_2)^{-1}$ layer also contributes to the conductivity of the system. These metallic O 2p states are mainly induced by the oxygen dangling bonds on the surface. Figure 2b demonstrates that the interfacial metallicity is caused by fully spin-polarized Ti $3d_{xy}$ states from the first $TiO_2$ layer (IF-I), along with a small contribution from the third $TiO_2$ layer (IF-III). It is also noticed that both the $d_{xy}$ and $d_{yz}$ orbitals from Ti atoms of the third layer (IF-III) contribute to some metallic states, although their contribution is small. This means that when charge transfers to deeper layers of the STO substrate more $d_{yz}/d_{xz}$ orbitals contribute to the metallic states. Furthermore, Figure 2b shows that O $2p_x/p_y$ orbitals from the $AlO_2$ surface layer also take part in the formation of metallic states, which is consistent with the previous results.[4,42] A direct view of the contributions to the metallic states from the O 2p and Ti 3d orbitals can be seen from the three-dimensional charge density in Figure 2a. It clearly shows that all these O 2p orbitals on the surface and the Ti 3d orbitals at the interface contribute to the charge density that forms the metallic states. Moreover, the charge density plot shows that the $d_{yz}/d_{xz}$ character-like orbitals from the IF-III layer substantially participate in the conductivity, along with the $d_{xy}$ orbital, which is consistent with the calculated orbital-resolved partial DOS in Figure 2b. In short, the metallicity in this system mostly comes from partial occupation of Ti $3d_{xy}$ orbitals at the interfacial region and O $2p_x/p_y$ orbitals at the surface layer. However, it is noticed that the hole states induced by surface O 2p states may be neutralized by the oxygen vacancies on the surface, and if so, only the *n*-type interfacial conductivity can be observed.[9] In summary, when the thickness of the LAO film gradually increases from 1 layer to 5 layers, the HS-based slab system shows the following trends: (1) The O 2p states of the LAO film gradually shift toward higher energy, decreasing the band gap energies to zero. (2) The polar discontinuity between LAO and STO will produce an increasing driving force to transfer electrons from the LAO layers to the STO substrate, and these transferred electrons will partially occupy Ti 3d orbitals and form interfacial metallic states.

**3.3. Critical Thickness for Forming 2DEG in Strained HS.** Next, we studied the influence of biaxial compressive and tensile strain on the 2DEG of the LAO/STO HS-based slab system. The biaxial strain within the STO substrate was modeled by modifying its lattice parameters in the *ab*-plane. The experimental lattice parameter of STO, 3.905 Å, is used as a reference point (0% strain in *ab*-plane) and is then adjusted from −1.5% to +1.5%. The "−" and "+" signs indicate compressive and tensile strains, respectively. In order to see the changes in electronic states induced by the biaxial strain in STO, we calculated the total DOS of the $(LAO)_n$/STO (001) ($n = 4$, 5, and 6) systems with strains of −1.5%, −1%, +1%, and +1.5%, as illustrated in Figure 3. The first, second, and third rows represent $(LAO)_4$/STO, $(LAO)_5$/STO, and $(LAO)_6$/STO HS-based slab systems, respectively. Our calculated total DOS indicates that all the strained $(LAO)_4$/STO HS systems show semiconducting behavior in the range between −1.5% and +1.5% (first row in Figure 3). These results are identical to that of the unstrained slab system. However, its band gap decreases as the strain on the substrate is adjusted from tensile to compressive. Similarly, the $(LAO)_5$/STO system with −1%, +1%, and +1.5% strains also shows a semiconducting nature (second row in Figure 3). However, a very small amount of states are still present at the Fermi level for the −1.5% strained system, and thus the system exhibits weak metallicity. Considering that there exists a critical thickness for the LAO film for forming 2DEG and that a thin LAO film may lead to insulating behavior, one may speculate that the energy gap in the −1%, +1%, and +1.5% strained systems could be closed by increasing the thickness of the LAO film. To verify this hypothesis, we modeled the $(LAO)_6$/STO system and calculated its electronic structure. The total DOS for the $(LAO)_6$/STO system with −1.5%, −1%, +1%, and +1.5% strains is shown in the third row of Figure 3. It shows that the $(LAO)_6$/STO systems exhibit metallic natures and that more states arise near the Fermi level as the strain on the STO substrate is adjusted from compressive to tensile. In short, our calculations yield the following conclusions: (1) For the unstrained LAO/STO HS-based slab system, as mentioned before, 5 unit cells of the LAO film is the minimum critical

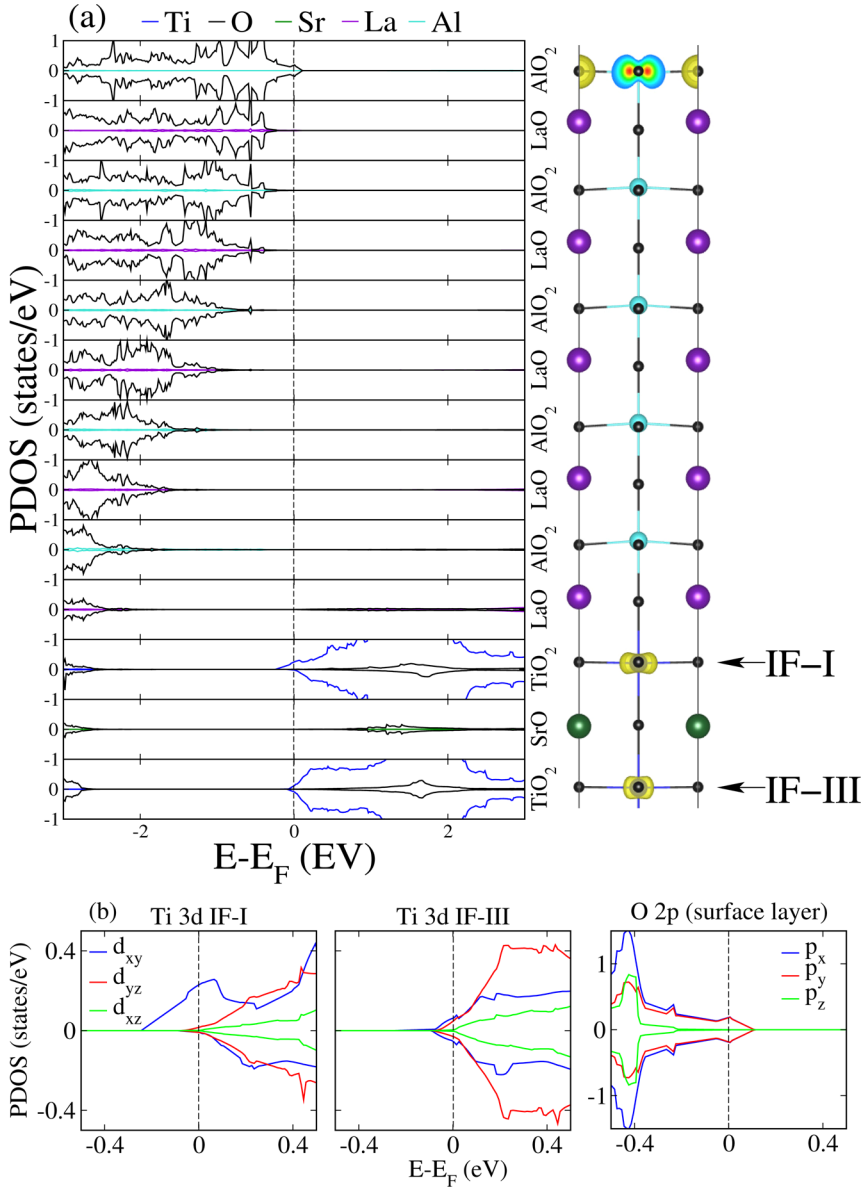


**Figure 2.** (a) Calculated spin-polarized partial DOS projected on different layers for the unstrained $(LAO)_5$/STO HS-based slab model, along with the charge density plot calculated in the energy range from −0.3 to 0 eV. (b) Orbital-resolved partial DOS for Ti atoms at the first (IF-I) and third (IF-III) $TiO_2$ layers and for O atoms at the surface $AlO_2$ layer.

thickness to obtain a 2DEG.[6,8] (2) For the compressively strained systems within −1.5%, a critical thickness of 5 to 6 unit cells of LAO is still required, but the system shows relatively low interfacial charge carrier density. As discussed later, this is because the charge transferred from LAO layers extends into deep STO layers, which dilutes the interfacial charge density. (3) For the tensilely strained systems within +1.5%, our calculations show that 6 unit cells of LAO are the minimum requirement to form a 2DEG. These results indicate that biaxial strain applied on the STO (001) substrate in the *ab*-plane has a profound impact on the critical thickness of a LAO film for forming the 2DEG.

To deeply understand how the electronic properties evolve with various biaxial strains, we produced the layer-resolved Ti 3d DOS of $(LAO)_6$/STO HS-based slab systems with −1.5%, −0.5%, +0.5%, and +1.5% biaxial strains on the STO substrate in Figure 4a, 4b, 4c, and 4d, respectively. The projected Ti 3d orbitals from three consecutive interfacial $TiO_2$ layers in the STO substrate were extracted. The first, third, and fifth $TiO_2$ layers of STO were defined as IF-I, IF-III, and IF-V, respectively. Our results indicate that when the STO substrate undergoes a strain from −1.5% to +1.5% the density of interfacial (IF-I) Ti 3d states near the Fermi level increases. The −1.5% compressively strained system (Figure 4a) shows the least Ti 3d states near the Fermi level, while the system with +1.5% tensile strain (Figure 4d) shows the most. This means that the interfacial charge carrier density will increase when a large tensile strain is applied on the STO substrate. According to crystal field theory, the Ti 3d states in the regular octahedral crystal field are split into triply degenerate $t_{2g}$ ($d_{xy}$, $d_{xz}$, and $d_{yz}$) and doubly degenerate $e_g$ ($d_{3z^2-r^2}$ and $d_{x^2-y^2}$) states. The $TiO_6$ unit in the relaxed HSs, however, is distorted. This distortion degrades the symmetry of the $TiO_6$ unit, and the triply degenerate $t_{2g}$ states are further split into nondegenerate $d_{xy}$, $d_{xz}$, and $d_{yz}$ orbitals. To examine the Ti 3d splitting behavior under various strains, we calculated the orbital-resolved DOS at


dx.doi.org/10.1021/am506336w | ACS Appl. Mater. Interfaces 2014, 6, 22351−22358

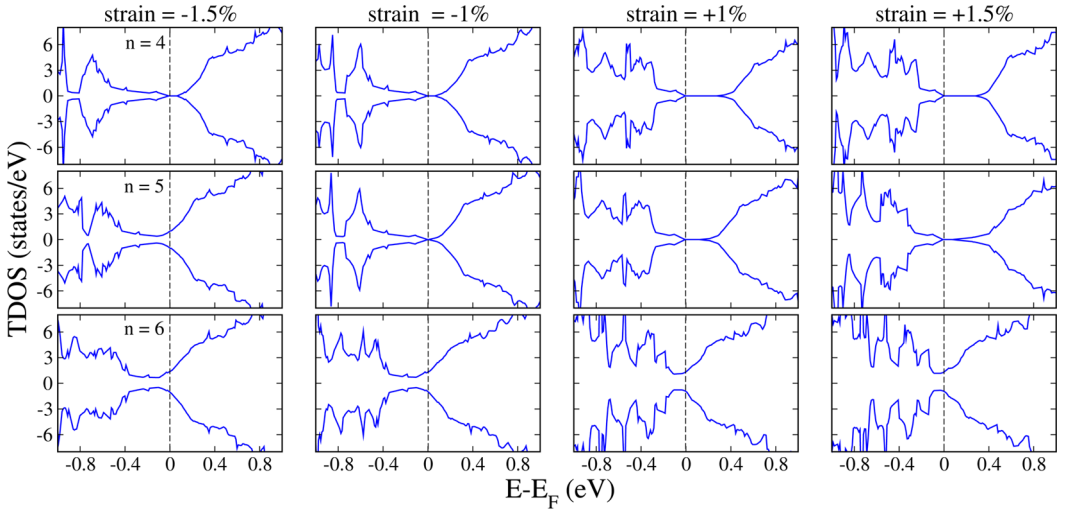


**Figure 3.** Calculated spin-polarized total DOS of $(LAO)_n/STO$ ($n$ = 4, 5, and 6) HS-based slab systems for −1.5%, −1%, +1%, and +1.5 biaxial strain on STO substrates in the *ab*-plane. The "−" and "+" signs indicate compressive and tensile strains, respectively. A critical thickness of 6 LAO unit cells is found for metallicity in the strained systems from −1% to +1.5%.

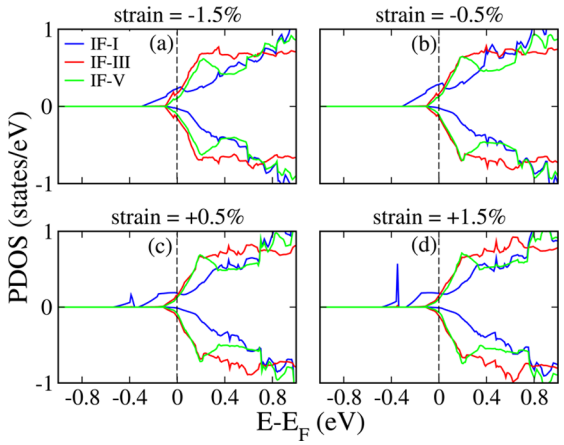


**Figure 4.** Calculated Ti 3d layer-resolved DOS of the $(LAO)_6/STO$ HS-based slab systems with −1.5% (a), −0.5% (b), +0.5% (c), and +1.5% (d) biaxial strains on the STO substrate in the *ab*-plane. The IF-I, IF-III, and IF-V stand for the first, third, and fifth $TiO_2$ layers of the STO substrate, respectively.

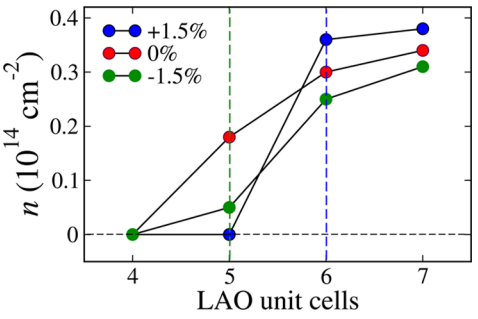


**Figure 5.** Calculated charge carrier density of Ti 3d orbitals from interfacial $TiO_2$ layers with respect to LAO unit cells for −1.5%, 0%, and +1.5% strains at LAO/STO HS-based slab systems. The vertical green and blue dashed lines represent the critical thickness of LAO thin films for strained systems to form 2DEG.

the IF-I $TiO_2$ layer for different strained systems, as shown in the Supporting Information. Our calculation clearly indicates that $d_{xy}$ states are primarily responsible for the interfacial conductivity in each case and that the $d_{xy}$ orbital occupation increases near the Fermi energy as the strain increases from −1.5% to +1.5%. In contrast, the $d_{yz}$ and $d_{xz}$ states remain unoccupied and do not contribute to the interfacial conductivity.

**3.4. Interfacial Charge Carrier Density and Magnetism.** Since the interfacial metallic states play a major role in determining the conductivity of the LAO/STO system,[10] to obtain a qualitative comparison of the charge carrier density with respect to LAO film thickness for various strained systems, we computed the partial occupation of Ti 3d orbitals from interfacial $TiO_2$ (IF-I) by integrating the partial DOS of the electron occupied states near the Fermi level. The calculated charge carrier densities of Ti 3d orbitals for $(LAO)_n$ ($n$ = 4, 5, 6, and 7) thin films on the STO(001) substrate are plotted in Figure 5, for −1.5%, 0%, and +1.5% strained HSs. The charge carrier density values show a significant interdependence with LAO unit cells and lattice strains. For $(LAO)_4/STO$ HSs, all the strained slab systems give a zero charge carrier density. For $(LAO)_5/STO$ HS, the −1.5% compressively strained system gives a minimum Ti 3d charge carrier density. When the LAO film increases up to 6 unit cells, all the strained systems exhibit conducting behavior. Moreover, a maximum charge carrier density is obtained for the $(LAO)_7/STO$ system. In addition, it is also noted that in conducting HS systems with the same LAO unit cells such as the $(LAO)_6/STO$ model the interfacial charge carrier density increases when a biaxial strain ranging from −1.5% to +1.5% is applied on the STO substrate.

In addition, we found that the magnetic moment of the Ti atom on the interface also shows an increasing trend when the STO substrate undergoes a strain from −1.5% to +1.5%. The magnetic moment of the Ti atom in the IF-I layer increases from 0.05 $\mu_B$ to 0.09 $\mu_B$ in the $(LAO)_6/STO$ system and from 0.07 $\mu_B$ to 0.10 $\mu_B$ in the $(LAO)_7/STO$ slab system. A tiny magnetic moment of 0.02 $\mu_B$ and 0.04 $\mu_B$ is also observed at Ti atoms in the second $TiO_2$ (IF-III) layers for −1.5% compressively strained $(LAO)_6/STO$ and $(LAO)_7/STO$ systems, respectively. This is because a small amount of charge is transferred from polar $(LaO)^{+1}$ to deeper $TiO_2$ layers within the STO substrate. In short, our theoretical calculations reveal that the STO-based slab systems with *ab*-plane strains on the


dx.doi.org/10.1021/am506336w | ACS Appl. Mater. Interfaces 2014, 6, 22351−22358

substrate increase the critical thickness of LAO film for forming 2DEG. For metallic LAO/STO HS systems, the orbital occupation of Ti 3d states at the interfacial layer increases when the STO substrate undergoes a large tensile strain, thus leading to higher charge carrier density and elevated magnetic moments. However, it is also noted that the calculated magnetic moments in the LAO/STO HS-based slab system (with vacuum layer) are much smaller than that in the periodic LAO/STO HS system (without a vacuum layer). For a periodic LAO/STO HS system, about $0.5e^-$ is transferred from LAO to the STO substrate due to the polar discontinuity. The $0.5e^-$ will occupy partially occupied Ti 3d orbitals and thus lead to a total magnetic moment of about 0.5 $\mu_B$.[23] For LAO/STO HS-based slab systems, there exist two polar discontinuities, one at the interface and another one at the $(AlO_2)^-$ surface. The existence of a bare surface $(AlO_2)^-$ layer inhibits the charge transfer from the LAO to STO, and thus, with respect to the periodic LAO/STO HS system, fewer electrons are transferred to STO, leading to relatively small magnetic moments. Actually, using the GGA+$U$ approach, Pavlenko et al. also obtained a relatively small magnetic moment of about 0.005 $\mu_B$ for the interfacial Ti ion in the LAO/STO HS-based slab system.[43] Interestingly, the calculated smaller magnetic moment in the HS-based slab system is well consistent with the experimentally observed value that is smaller than $10^{-3}\mu_B$/Ti in the oxygen-annealed LAO/STO system (without oxygen vacancies).[44] However, Pavalenko et al. also pointed out that the oxygen vacancy could enhance the magnetic moment up to 0.34 $\mu_B$, which is in good agreement with the recent experimental value of about 0.3 $\mu_B$ in the oxygen-deficient LAO/STO system.[45]

### 3.5. Origin of the Interfacial and Surface Metallicity.

To deeply understand the behavior of the metallic states at the interface and surface layers with respect to the degree of the strain, we plotted the charge density projected on the bands forming the 2DEG for the $(LAO)_6$/STO HS slab system in Figure 6. This is because we had previously confirmed that, for strained LAO/STO HSs, 6 unit cells of LAO thin films are necessary to produce the 2DEG. Figure 6a, 6b, 6c, 6d, and 6e represents the −1.5%, −1%, 0%, +1%, and +1.5% strained systems, respectively. The results show that, when a compressive strain is applied on the STO substrate, electrons transferred from the polar $(LaO)^{+1}$ layer extend to the deeper $(TiO_2)^0$ layers of the STO substrate. This indicates that the metallic region extends deep into STO along the $c$-axis, which weakens the quantum confinement effects of the 2DEG. This also leads to the decrease of the interfacial charge carrier density and magnetic moments. In contrast, when a tensile strain is applied on the STO substrate, electrons transferred to the STO substrate are mainly confined at $TiO_2$ layers near the interfacial region. In particular, for HS systems with a tensile strain $n \geq +1.5\%$, the interfacial metallicity is completely caused by the Ti atoms on the IF-I layer, which makes it form an ideal 2DEG. Interestingly, O 2p states near the Fermi level belonging to the surface layer show the opposite trend to the interface states with respect to the strain. As the STO substrate undergoes from −1.5% compressive to +1.5% tensile strain, the metallic region spans to deeper layers of LAO unit cells (see Figure 6). For −1.5% compressively strained systems, only O 2p states from the outermost $AlO_2$ layer contribute to the surface conductivity, while for +1.5% tensilely strained systems the surface metallic states extend up to 2.5 unit cells of LAO.

To study the electronic structure evolution of the O 2p orbitals near the surface region with strain, we plotted the orbital-resolved O 2p DOS of $(LAO)_6$/STO for various strains in Figure 7. The first row represents the surface $AlO_2$ layers,

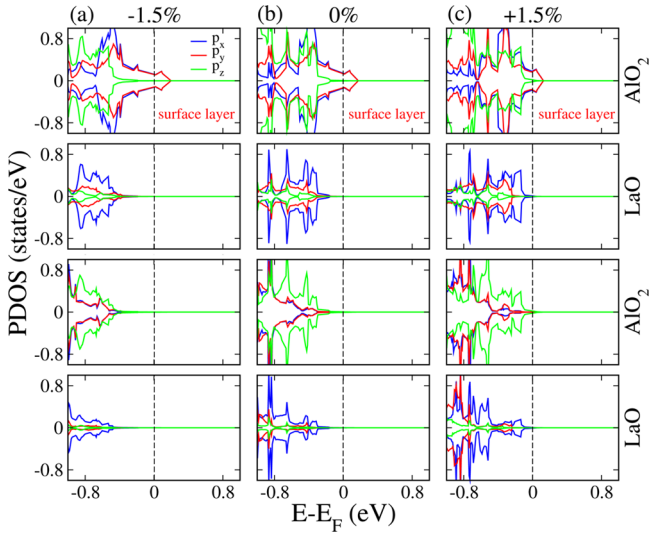


**Figure 7.** Orbital-resolved partial DOS of O 2p orbitals projected on different $AlO_2$ layers for $(LAO)_6$/STO HS-based slab systems with −1.5% (a), 0% (b), and +1.5% (c) strains.

where O $2p_x/p_y$ orbitals cross the Fermi level, showing metallic properties. In contrast, O 2p orbitals in the deeper LAO layers have no contribution to the surface metallicity. From the DOS plot, one can explicitly find that, when the system undergoes a strain from −1.5% to +1.5%, more hole states emerge at the $AlO_2$ surface layers, and the O 2p states in the deeper LAO thin films significantly shift toward higher energy (see Figure 7b and 7c). For the +1.5% tensilely strained system, O 2p orbitals from deep LAO layers shift toward the Fermi level and partially contribute the surface metallicity. This can also be observed from the charge density plot in Figure 6e. In summary, in contrast with the interfacial metallic states, for the −1.5% compressively strained system, the surface metallic states are

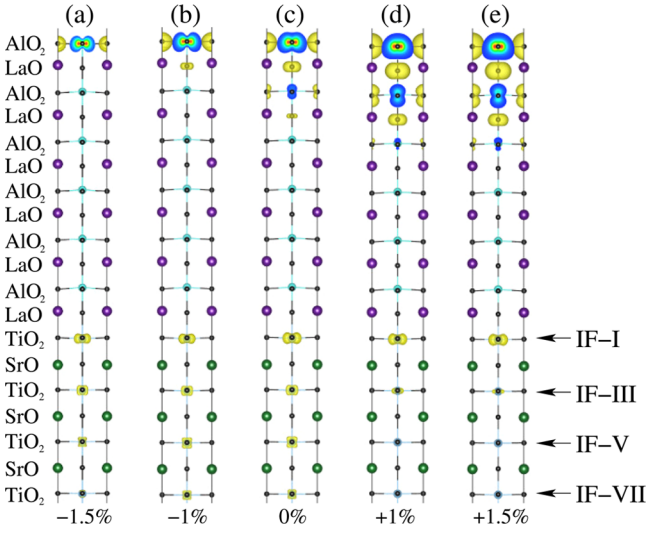


**Figure 6.** Charge density projected on the bands forming the metallic states near the interface and surface region in the $(LAO)_6$/STO HS-based slab systems with −1.5% (a), −1% (b), 0% (c), +1% (d), and +1.5% (e) strains.

tightly confined in the surface $AlO_2$ layer, while for the +1.5% tensilely strained system, the surface metallic states extend up to 1.5 unit cells of LAO. Moreover, in the second $AlO_2$ layer, more O $2p_z$ character-like bands emerge near the Fermi level (energy range from −0.3 to 0 eV) as the system undergoes a tensile strain from 0% to +1.5%. This trend is consistent with the charge density distribution.

Finally, to investigate the energy shift of O 2p states in the LAO thin film with various strains, we calculated the electrostatic potential along the *c*-direction (perpendicular to the interface) of $(LAO)_6$/STO for −1.5%, 0%, and +1.5% strained systems, as illustrated in Figure 8. It clearly indicates

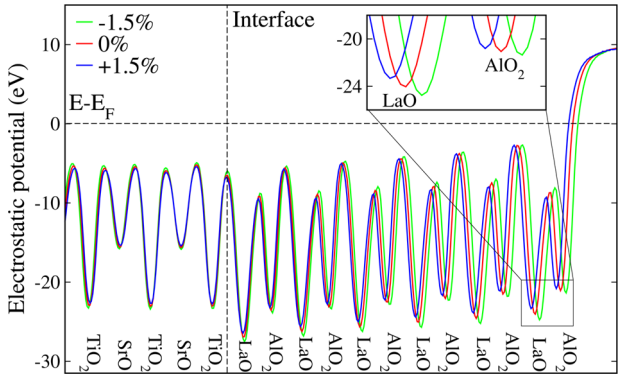


**Figure 8.** Calculated electrostatic potential of the $(LAO)_6$/STO HS-based slab systems with −1.5%, 0%, and +1.5% strains along the *c*-axis and averaged over the *ab*-plane. The inset shows the enlarged potential of the layers close to the vacuum layer.

that electrostatic potential of the LAO thin film gradually increases layer by layer toward the vacuum. This makes the valence band of the surface LAO layers move toward the Fermi level, and eventually, the O 2p orbitals in the surface $AlO_2$ layer cross the Fermi level, forming metallic states.[29] To explicitly show the strain effects on the electrostatic potential, we magnified the electrostatic potential of the LAO layers near the vacuum (see the inset in Figure 8), which illustrates that the electrostatic potential value is higher for tensilely strained systems than that for compressively strained systems. For the −1.5%, 0%, and +1.5% strained systems, the calculated electrostatic potential values are about −21.45, −21.18, and −20.79 eV for the surface $AlO_2$ layer and −24.48, −24.07, and −23.39 eV for the LaO layer, respectively. This means that the valence band edge of O 2p states moves toward high energy in tensilely strained systems and low energy in the compressively strained systems, respectively.

## 4. CONCLUSIONS

In conclusion, the electronic and magnetic properties of unstrained and strained LAO/STO HS-based slab systems are studied using spin-polarized density functional theory calculations. It is found that a critical thickness of 5 LAO unit cells is required for forming 2DEG states in the unstrained LAO/STO slab system, while the critical thickness of LAO thin film increases up to 6 unit cells in both the compressively and tensilely strained systems within the range between −1.5% and +1.5%. For the metallic HS-based slab system such as $(LAO)_6$/STO, when the STO substrate undergoes a strain from compressive to tensile, the surface conducting hole states become delocalized and extend to deep LAO layers, but in contrast, the interfacial metallic electron states become localized and tightly confined within the interfacial $TiO_2$ layer. We suggest that the *n*-type interfacial charge carrier density and magnetic moment of the STO-based HS systems can be optimized by applying a tensile strain on the STO substrate along the *ab*-plane.

## ■ ASSOCIATED CONTENT

### Supporting Information

Calculated Ti 3d orbital-resolved DOS at *n*-type IF-I $TiO_2$ layer of the $(LAO)_6$/STO HS-based slab systems with various biaxial strain on the STO substrate in the *ab*-plane. This material is available free of charge via the Internet at http://pubs.acs.org.

## ■ AUTHOR INFORMATION

### Corresponding Author

*E-mail: kesong@ucsd.edu. Phone: +1-858-534-2514.

### Notes

The authors declare no competing financial interest.

## ■ ACKNOWLEDGMENTS

The authors thank Maziar Behtash and Camille Bernal for useful discussions. This work is partially supported by ONR (N000141510030). KY acknowledges support by start-up funds from the University of California, San Diego.

## ■ REFERENCES

(1) Ohtomo, A.; Hwang, H. Y. A High-Mobility Electron Gas at the $LaAlO_3/SrTiO_3$ Heterointerface. *Nature* **2004**, *427*, 423−426.
(2) Brinkman, A.; Huijben, M.; van Zalk, M.; Huijben, J.; Zeitler, U.; Maan, J. C.; van der Wiel, W. G.; Rijnders, G.; Blank, D. H. A.; Hilgenkamp, H. Magnetic Effects at the Interface between Non-Magnetic Oxides. *Nat. Mater.* **2007**, *6*, 493−496.
(3) Ariando; Wang, X.; Baskaran, G.; Liu, Z. Q.; Huijben, J.; Yi, J. B.; Annadi, A.; Barman, A. R.; Rusydi, A.; Dhar, S.; Feng, Y. P.; Ding, J.; Hilgenkamp, H.; Venkatesan, T. Electronic Phase Separation at the $LaAlO_3/SrTiO_3$ Interface. *Nat. Commun.* **2010**, *2*, 188−194.
(4) Lesne, E.; Reyren, N.; Doennig, D.; Mattana, R.; Jaffrés, H.; Cros, V.; Choueikani, F. .; Ohresser, P.; Pentcheva, R.; Barthélémy, A.; Bibes, M. Suppression of the Critical Thickness Threshold for Conductivity at the $LaAlO_3/SrTiO_3$ Interface. *Nat. Commun.* **2012**, *5*, 4291.
(5) Mannhart, J.; Schlom, D. G. Oxide Interfaces-An Opportunity for Electronics. *Science* **2010**, *327*, 1607−1611.
(6) Pentcheva, R.; Pickett, W. E. Avoiding the Polarization Catastrophe in $LaAlO_3$ Overlayers on $SrTiO_3$(001) through Polar Distortion. *Phys. Rev. Lett.* **2009**, *102*, 107602.
(7) Salluzzo, M.; Cezar, J. C.; Brookes, N. B.; Bisogni, V.; De Luca, G. M.; Richter, C.; Thiel, S.; Mannhart, J.; Huijben, M.; Brinkman, A.; Rijnders, G.; Ghiringhelli, G. Orbital Reconstruction and the Two-Dimensional Electron Gas at the $LaAlO_3/SrTiO_3$ Interface. *Phys. Rev. Lett.* **2009**, *102*, 166804.
(8) Cossu, F.; Schwingenschlögl, U.; Eyert, V. Metal-Insulator Transition at the $LaAlO_3/SrTiO_3$ Interface Revisited: A Hybrid Functional Study. *Phys. Rev. B* **2013**, *88*, 045119.
(9) Cen, C.; Thiel, S.; Hammerl, G.; Schneider, C. W.; Andersen, K. E.; Hellberg, C. S.; Mannhart, J.; Levy, J. Nanoscale Control of an Interfacial Metal-Insulator Transition at Room Temperature. *Nat. Mater.* **2008**, *7*, 298−302.
(10) Cen, C.; Thiel, S.; Mannhart, J.; Levy, J. Oxide Nanoelectronics on Demand. *Science* **2009**, *323*, 1026−1030.
(11) Gozar, A.; Logvenov, G.; Kourkoutis, L. F.; Bollinger, A. T.; Giannuzzi, L. A.; Muller, D. A.; Bozovic, I. High-Temperature Interface Superconductivity between Metallic and Insulating Copper Oxides. *Nature* **2008**, *455*, 782−785.

(12) Sato, H.; Tsukada, A.; Naito, M.; Matsuda, A. $La_{2-x}Sr_xCuO_y$ Epitaxial Thin Films ($x$ = 0 to 2): Structure, Strain, and Superconductivity. *Phys. Rev. B* **2000**, *61*, 12447.
(13) Warusawithana, M. P.; Cen, C.; Sleasman, C. R.; Woicik, J. C.; Li, Y.; Kourkoutis, L. F.; Klug, J. A.; Li, H.; Ryan, P.; Wang, L. P.; Bedzyk, M.; Muller, D. A.; Chen, L. Q.; Levy, J.; Schlom, D. G. A Ferroelectric Oxide Made Directly on Silicon. *Science* **2009**, *324*, 367−370.
(14) Choi, K. J.; Biegalski, M.; Li, Y. L.; Sharan, A.; Schubert, J.; Uecker, R.; Reiche, P.; Chen, Y. B.; Pan, X. Q.; Gopalan, V.; Chen, L. Q.; Schlom, D. G.; Eom, C. B. Enhancement of Ferroelectricity in Strained $BaTiO_3$ Thin Films. *Science* **2004**, *306*, 1005−1009.
(15) Haeni, J. H.; Irvin, P.; Chang, W.; Uecker, R.; Reiche, P.; Li, Y. L.; Choudhury, S.; Tian, W.; Hawley, M. E.; Craigo, B.; Tagantsev, A. K.; Pan, X. Q.; Streiffer, S. K.; Chen, L. Q.; Kirchoefer, S. W.; Levy, J.; Schlom, D. G. Room-Temperature Ferroelectricity in Strained $SrTiO_3$. *Nature* **2004**, *430*, 758−761.
(16) Wen, Z.; Qiu, X.; Li, C.; Zheng, C.; Ge, X.; Li, A.; Wu, D. Mechanical Switching of Ferroelectric Polarization in Ultrathin $BaTiO_3$ Films: The Effects of Epitaxial Strain. *Appl. Phys. Lett.* **2014**, *104*, 042907−042911.
(17) Yang, K.; Setyawan, W.; Wang, S.; Nardelli, M. B.; Curtarolo, S. A Search Model for Topological Insulators with High-Throughput Robustness Descriptors. *Nat. Mater.* **2012**, *11*, 614−619.
(18) Berger, R. F.; Fennie, C. J.; Neaton, J. B. Band Gap and Edge Engineering via Ferroic Distortion and Anisotropic Strain: The Case of $SrTiO_3$. *Phys. Rev. Lett.* **2011**, *107*, 146804.
(19) Welser, J.; Hoyt, J. L.; Gibbons, J. F. Electron Mobility Enhancement in Strained-Si n-type Metal-Oxide-Semiconductor Field-Effect Transistors. *IEEE Electron Device Lett.* **1994**, *15*, 100−102.
(20) Jalan, B.; Allen, S. J.; Beltz, G. E.; Moetakef, P.; Stemmer, S. Enhancing the Electron Mobility of $SrTiO_3$ with Strain. *Appl. Phys. Lett.* **2011**, *98*, 132102−132104.
(21) Chu, M.; Sun, Y.; Aghoram, U.; Thompson, S. E. Strain: A Solution for Higher Carrier Mobility in Nanoscale MOSFETs. *Annu. Rev. Mater. Res.* **2009**, *39*, 203−229.
(22) Bark, C. W.; Felker, D. A.; Wang, Y.; Zhang, Y.; Jang, H. W.; Folkman, C. M.; Park, J. W.; Baek, S. H.; Zhou, H.; Fong, D. D.; Pan, X. Q.; Tsymbal, E. Y.; Rzchowski, M. S.; Eom, C. B. Tailoring a Two-Dimensional Electron Gas at the $LaAlO_3/SrTiO_3$ (001) Interface by Epitaxial Strain. *Proc. Natl. Acad. Sci. U.S.A.* **2011**, *108*, 4720−4724.
(23) Nazir, S.; Behtash, M.; Yang, K. Enhancing Interfacial Conductivity and Spatial Charge Confinement of $LaAlO_3/SrTiO_3$ Heterostructures via Strain Engineering. *Appl. Phys. Lett.* **2014**, *105*, 141602−141605.
(24) Thiel, S.; Hammerl, G.; Schmehl, A.; Schneider, C. W.; Mannhart, J. Tunable Quasi-Two-Dimensional Electron Gases in Oxide Heterostructures. *Science* **2006**, *313*, 1942−1945.
(25) Asmara, T. C.; Annadi, A.; Santoso, I.; Gogoi, P. K.; Kotlov, A.; Omer, H. M.; Motapothula, M.; Breese, M. B. H.; Rübhausen, M.; Venkatesan, T.; Ariando; Rusydi, A. Mechanisms of Charge Transfer and Redistribution in $LaAlO_3/SrTiO_3$ Revealed by High-Energy Optical Conductivity. *Nat. Commun.* **2014**, *5*, 3663.
(26) Kresse, G.; Furthmüller, J. Efficient Iterative Schemes for *Ab-Initio* Total-Energy Calculations Using a Plane-Wave Basis Set. *Phys. Rev. B* **1996**, *54*, 11169−11186.
(27) Kresse, G.; Furthmüller, J. Efficiency of *Ab-Initio* Total Energy Calculations for Metals and Semiconductors Using a Plane-Wave Basis Set. *Comput. Mater. Sci.* **1996**, *6*, 15−50.
(28) Perdew, J. P.; Burke, K.; Ernzerhof, M. Generalized Gradient Approximation Made Simple. *Phys. Rev. Lett.* **1996**, *77*, 3865−3868.
(29) Yang, X.; Su, H. Polarization and Electric Field Dependence of Electronic Properties in $LaAlO_3/SrTiO_3$ Heterostructures. *ACS Appl. Mater. Interfaces* **2011**, *3*, 3819−3823.
(30) Yang, K.; Dai, Y.; Huang, B.; Feng, Y. P. First-Principles GGA +$U$ Study of the Different Conducting Properties in Pentavalent-Ion-Doped Anatase and Rutile $TiO_2$. *J. Phys. D: Appl. Phys.* **2014**, *47*, 275101.
(31) Yang, K.; Dai, Y.; Huang, B.; Feng, Y. P. Density Functional Characterization of the Antiferromagnetism in Oxygen-Deficient Anatase and Rutile $TiO_2$. *Phys. Rev. B* **2010**, *81*, 033202.
(32) Okamoto, S.; Millis, A. J.; Spaldin, N. A. Lattice Relaxation in Oxide Heterostructures: $LaTiO_3/SrTiO_3$ Superlattices. *Phys. Rev. Lett.* **2006**, *97*, 056802.
(33) Hamann, D. R.; Muller, D. A.; Hwang, H. Y. Lattice-Polarization Effects on Electron-Gas Charge Densities in Ionic Superlattices. *Phys. Rev. B* **2006**, *73*, 195403.
(34) Pentcheva, R.; Pickett, W. E. Ionic Relaxation Contribution to the Electronic Reconstruction at the $n$-type $LaAlO_3/SrTiO_3$ Interface. *Phys. Rev. B* **2008**, *78*, 205106.
(35) Popović, Z. S.; Satpathy, S.; Martin, R. M. Origin of the Two-Dimensional Electron Gas Carrier Density at the $LaAlO_3$ on $SrTiO_3$ Interface. *Phys. Rev. Lett.* **2008**, *101*, 256801.
(36) Pavlenko, N.; Kopp, T. Structural Relaxation and Metal-Insulator Transition at the Interface between $SrTiO_3$ and $LaAlO_3$. *Surf. Sci.* **2011**, *605*, 1114−1121.
(37) Salluzzo, M.; Gariglio, S.; Torrelles, X.; Ristic, Z.; Di Capua, R.; Drnec, J.; Sala, M. M.; Ghiringhelli, G.; Felici, R.; Brookes, N. B. Structural and Electronic Reconstructions at the $LaAlO_3/SrTiO_3$ Interface. *Adv. Mater.* **2013**, *25*, 2333−2338.
(38) Pauli, S. A.; Leake, S. J.; Delley, B.; Björck, M.; Schneider, C. W.; Schlepütz, C. M.; Martoccia, D.; Paetel, S.; Mannhart, J.; Willmott, P. R. Evolution of the Interfacial Structure of $LaAlO_3$ on $SrTiO_3$. *Phys. Rev. Lett.* **2011**, *106*, 036101.
(39) Lee, J.; Demkov, A. A. Charge Origin and Localization at the $n$-type $SrTiO_3/LaAlO_3$ Interface. *Phys. Rev. B* **2008**, *78*, 193104.
(40) Sing, M.; Berner, G.; GoB, K.; Müller, A.; Ruff, A.; Wetscherek, A.; Thiel, S.; Mannhart, J.; Pauli, S. A.; Schneider, C. W.; Willmott, P. R.; Gorgoi, M.; Schäfers, F.; Claessen, R. Profiling the Interface Electron Gas of $LaAlO_3/SrTiO_3$ Heterostructures with Hard X-Ray Photoelectron Spectroscopy. *Phys. Rev. Lett.* **2009**, *102*, 176805.
(41) Ristic, Z.; Di Capua, R.; Chiarella, F.; De Luca, G. M.; Maggio-Aprile, I.; Radovic, M.; Salluzzo, M. Photodoping and In-Gap Interface States across the Metal-Insulator Transition in $LaAlO_3/SrTiO_3$ Heterostructures. *Phys. Rev. B* **2012**, *86*, 045127.
(42) You, J. H.; Lee, J. H. Critical Thickness for the Two-Dimensional Electron Gas in $LaTiO_3/SrTiO_3$ Superlattices. *Phys. Rev. B* **2013**, *88*, 155111.
(43) Pavlenko, N.; Kopp, T.; Tsymbal, E. Y.; Sawatzky, G. A.; Mannhart, J. Magnetic and Superconducting Phases at the $LaAlO_3/SrTiO_3$ Interface: The Role of Interfacial Ti 3$d$ Electrons. *Phys. Rev. B* **2012**, *85*, 020407.
(44) Salluzzo, M.; Gariglio, S.; Stornaiuolo, D.; Sessi, V.; Rusponi, S.; Piamonteze, C.; De Luca, G. M.; Minola, M.; Marré, D.; Gadaleta, A.; Brune, H.; Nolting, F.; Brookes, N. B.; Ghiringhelli, G. Origin of Interface Magnetism in $BiMnO_3/SrTiO_3$ and $LaAlO_3/SrTiO_3$ Heterostructures. *Phys. Rev. Lett.* **2013**, *111*, 087204.
(45) Li, L.; Richter, C.; Mannhart, J.; Ashoori, R. C. Coexistence of Magnetic Order and Two-dimensional Superconductivity at $LaAlO_3/SrTiO_3$ Interfaces. *Nat. Phys.* **2011**, *7*, 762−766.